Heterozygous expression of the Alzheimer's disease protective PLCγ2 P522R variant enhances Aβ clearance while preserving synapses.

Shiden Solomon
King's College London Institute of Psychiatry Psychology and Neuroscience
Nirmal Kumar Sampathkumar
Oxford University: University of Oxford
Ivo Carre
King's College London Institute of Psychiatry Psychology and Neuroscience
Mrityunjoy Mondal
King's College London Institute of Psychiatry Psychology and Neuroscience
George Chennell
King's College London Institute of Psychiatry Psychology and Neuroscience
Anthony C. Vernon
King's College London Institute of Psychiatry Psychology and Neuroscience
Marc-David Ruepp
King's College London Institute of Psychiatry Psychology and Neuroscience
Jacqueline Mitchell (✉ jacqueline.mitchell@kcl.ac.uk)
King's College London Institute of Psychiatry Psychology and Neuroscience https://orcid.org/0000-0002-2677-398X

Research article

Keywords: Alzheimer's disease, Microglia, PLCG2, iPSC

Posted Date: March 25th, 2022

DOI: https://doi.org/10.21203/rs.3.rs-1420006/v1

Abstract

Background: A rare coding variant, *P522R,* in the phosphoplipase C gamme 2 (*PLCG2)* gene has been identified as protective against late onset Alzheimer's disease (AD), but the mechanism of protection is unknown. *PLCG2* is exclusively expressed in microglia within the central nervous sytem, and altered microglial function has increasingly been implicated in the progression of AD.

Methods: Healthy control hiPSCs were CRISPR edited to generate cells heterozygous and homozygous for the PLCG2^{P522R} variant. Microglia derived from these hiPSC's were used to investigate the impact of PLCg2^{P522R} on disease relevant processes, specifically microglial capacity to take up amyloid beta (Ab) and synapses. Targeted qPCR assessment was conducted to explore expression changes in core AD linked and microglial genes, and nitochondrial function was assessed using an Agilent Seahourse assay.

Results: Heterozygous expression of the *P522R* variant resulted in increased microglial clearance of Ab, while preserving synapses. This was associated with the upregulation of a number of genes, including the anti-inflammatory cytokine Il-10, and the synpase-linked CX3CR1, as well as alterations in mitochondrial function, and increased cellular motility. The protective capacity of PLCg2^{P522R} appeared crucially dependent on (gene) 'dose', as cells homozygous for the variant showed reduced synapse preservation, and a differential gene expression profile relative to heterozygous cells.

Conclusions: These findings suggest that PLCg2^{P522R} may result in increased surveillance by microglia, as well as priming them towards an anti-inflammatory state, with an increased capacity to respond to increasing energy demands, but highlights the delicate balance of this system, with increasing PLCg2^{P522R} 'dose' resulting in reduced beneficial impacts.

Background

Alzheimer's disease (AD) is a devastating neurodegenerative disorder that presents a significant and growing global socioeconomic burden. Although significant work has focused on understanding and modifying the disease process, the development of truly effective therapies has remained elusive.

Converging lines of evidence from human genetics, neuroimaging and *post-mortem* brain tissue studies suggest that microglia are major contributors to molecular and phenotypic changes, including synaptic loss and Aβ clearance, in the AD brain [1]. Microglia constantly survey the brain parenchyma for debris, apoptotic cells, aberrant misfolded proteins, and pathogens [2, 3]. Under normal physiological conditions, microglia also play a pivotal role in maintaining normal brain homeostasis, modulating synaptic strength and plasticity during development [3]. In the presence of pathological stimuli however, microglia undergo a morphological transformation from a highly ramified structure to a more ameboid reactive phenotype [4]. These "reactive" microglia are characterized by rapid proliferation and enhanced secretion of chemokines, cytokines, and immune mediators central to tissue repair and clearance of cellular debris [5]. Crucially, a subset of disease associated microglia (DAM) have been identified in neurodegenerative

disorders such as AD [6], with a profile unique to disease, highlighting the importance of these cells to the disease process.

GWAS studies have identified several novel risk associated coding variants for late-onset AD (LOAD), many of which are associated with microglial and immune function and further link these cells with AD pathogenesis. Among these identified polymorphic genes are rare coding variants in microglial-associated genes such as triggering receptor expressed on myeloid cell-2 (TREM2), ABI family member 3 (ABI3), and phospholipase C-gamma-2 (PLCG2) [7]. Specifically, a single nucleotide polymorphism (Pro522Arg; *P522R*) in the PLCG2 gene, which is almost exclusively expressed in microgliawithin the central nervous system (CNS), has been found to be protective against LOAD [8], further highlighting the importance of these cells in disease.

The protein product of PLCG2 (PLCγ2) is recruited to the cell membrane upon activation by tyrosine kinase and modulates immune signals impacting cell fate and function, both in the brain and periphery [9, 10]. Recent studies have identified PLCγ2 downstream of TREM2 signalling, modulating different microglial functions such as phagocytosis, lipid metabolism, survival and cytokine release [11, 12]. It also appears to play a role in TLR4 signalling idenpdent of its role in the TREM2 pathway (10), highlighting it's role in facilitating inflammatory responses. However, specifically, how the *P522R* protective variant modulates microglia activity to protect against AD related pathologic insult remains unclear.

In AD, dysregulation of Aβ clearance and microglia mediated synaptic pruning are two mechanisms by which microglia contribute to disease progression. Therefore, a crucial therapeutic strategy in AD, at least from microglia associated function, would be robust clearance of Aβ aggregates while sparing synapses. In this study we demonstrate that the heterozygous PLCγ2^{P522R} protective variant modulates microglia mediated Aβ and synaptosome uptake, which may underpin its protective nature *in vivo*. We show a potential impact of PLCγ2^{P522R} on microglia mitochondrial function and ATP production, which may contribute to maintenance of microglia metabolic fitness. Additionally, we report enhanced activation status, higher lysosomal activity, and increased motility in PLCγ2 microglia variants. Crucially, we also demonstrate that the protective capacity of the PLCγ2^{P522R} variant is ciritically linked to its dose, highlighting the need for a better understanding of the specific impact this variant has on microglial function, and how these pathways may be manipulated to improve outcomes in AD.

Methods

iPSC line and maintenance

hiPSC line BIONi10-C (Bio Sample ID: SAMEA3158050, ECACC ID:66540023) was purchased from EBiSC, which was deposited by Bioneer, and are available for research from European Collection of Authenticated Cell Cultures (ECACC). The PLCγ2 WT locus was authenticated through sequencing (Supplementary Table 1) and the PLCγ2^{HET} and PLCγ2^{HOM} hiPSC lines were generated on the parent BIONi10-C WT background inhouse using CRISPR editing. hiPSCs were cultured on Geltrex coated (100X)

(A1413202, Gibco) plates and maintained at 37^{o}C and 5% CO_2 in E8-Flex medium (A2858501, ThermoFisher).

Crispr Editing

In brief, to insert the P522R variant, BIONi010-C WT hiPSCs were dissociated to single cells using StemPro™ Accutase™ (A1110501, ThermoFisher). Cells were then seeded at 5X10^5 per well of a 6-well plate and incubated for 3–4 hrs to allow for attachment. sgRNA complex was prepared by mixing 100 µM stock of trcrRNA (1072532, IDT) and crRNA (sequence – CCTACAGAACTACATTTTGG), targeting exon 17 of the PLCγ2 locus, in equimolar concentration with 196 µL of nuclease free duplex-buffer (IDT) to a final volume of 200 µL and annealing at 95^{o}C for 5 minutes. At the same time, 1 µM stock Cas9 RNP was made by adding 1 µL of 62 µM Hi-Fi Cas9 RNP (1081060, IDT) to 61 µL of Opti-MEM™ (31985070, ThermoFisher**)**. 12 µL of sgRNA complex and 12 µL of Cas9 RNP were then mixed in 76 µL of Opti-MEM and incubate at room temperature for 5 min. In parallel, 4 µL of Lipofectamine™ Stem (STEM00008, ThermoFisher) and 96 µL of Opti-MEM were mixed and incubated for 10 min at room temperature to make the transfection mixture. 2 µg of donor plasmid and 500 ng of puromycin selection construct were added to the sgRNA:Cas9 (RNP) complex and transfection mixture to a final volume of 200 µL, and incubated for 10 mins. The medium on the plated cells was replaced with 2 mL of pre-warmed Opti-MEM supplemented with RevitaCell™ (100X) (A2644501, ThermoFisher) and transfection mix was added on top in a drop-wise manner before mixing gently through swirling the plate. Cells were left for four hours in the incubator before medium top-up with E8-flex supplemented with RevitaCell and then being left on overnight. Medium changes were performed until cells reached 70–80% confluency, whereafter, single cell selection with 0.25 µM Puromycin (A1113803, ThermoFisher) was done to isolate pure colonies. Single cell colonies were established, expanded and banked. To confirm conversion of 522P to 522R, DNA was extracted using DNeasy Blood & Tissue (69506, QIAGEN) and sent for sequencing (Eurofins Genomics) (sequencing primers are available in supplementary methods Table 1) and positive colonies were identified to be used in downstream assays.

Generation of iPSC derived microglia

Microglia-like cells were generated following Haenseler et al. (Haenseler et al., 2017). In brief, embryonic bodies (EBs) were formed through plating and spinning of 3X10^6 BIONi010-C (BINI-10) (WT, PLCG2^{HET} and PLCG2^{HOM}) at 300 g on an AggreWell 800 plate (34850, StemCell Technologies) in E8-Flex medium supplemented with 50 ng/ml BMP4 (120-05ET, Peprotech), 50 ng/ml VEGF (PHC9394, ThermoFisher) and 20 ng/ml SCF (300-07, PeproTech). 75% medium change per day was performed for 72 hours, after which EBs were transferred to a T75 flask and maintained in X-VIVO15 (BE02-060F, Lonza) supplemented with 25 ng/ml IL-3 (PHC0031, ThermoFisher), 100 ng/ml M-CSF (300 – 25, PeproTech), 2 mM Glutamax (35050061, ThermoFisher) and 0.055 mM β-mercaptoethanol (31350-010, ThermoFisher). Medium was topped up every week and after 4 weeks, emerging precursor cells were collected and differentiated to

microglia-like cells for 7-days in microglia medium consisting of 25 mL DMEM/F12 (11330032, ThermoFisher) and 25 mL Neurobasal Plus media (A3582901, ThermoFisher) supplemented with 100 ng/ml M-CSF (300 – 25, Peprotech), 100 ng/ml IL-34 (200 – 34, peprotech) and 10 ng/ml GM-CSF (300-03, Peprotech), 2 mM Glutamax (35050061, ThermoFisher), 0.05 5mM β-mercaptoethanol (31350, Life Technologies), and 0.25 µg/mL Insulin (I9278, Sigma).

Generation of iPSC derived cortical neurons

iPSC derived cortical neurons differentiation was adapted from Fernandopulle et al. (Fernandopulle et al., 2018), with slight modifications. In brief, BIONi010-C (BINI-10) iPSC cell lines ($PLCG2^{HET}$) were dissociated using accutase and seeded as single cells at a density of $5X10^5$ per well of a six-well plate. The cells were left to attach for 4 hrs. Cells were then transduced in a similar manner to the above protocol of PLCγ2 editing, but in this case using a CRISPR-cas9 RNP to stably integrate a doxycycline inducible NGN2 expression cassette (see supplementary methods - plasmids), into the CLYBL safe harbour site, allowing for the driving of cellular differentiation into cortical neurons. Double selection was performed using Blasticidine (100ng/mL) (Code) and mApple markers to identify positive colonies. iPSCs stably expressing NGN2 were then induced in DMEM/F12 with HEPES (11330032, ThermoFisher) supplemented with; N2 (1X) (17502048, ThermoFisher), NEAA (1X) (11140050, ThermoFisher), Glutamax (1X) (35050038, ThermoFisher) and doxycycline (2µg/ml) (D9891, Sigma). 72 hours post induction, the cells were transferred to P-D-L (product code) and Laminin (1:100 dilution in PBS) (23017015, ThermoFisher) coated plates and fed with Neurobasal Plus media (A3582901, ThermoFisher) supplemented with; B27 (50X) (17504044, ThermoFisher), 10 ug/ml BDNF (450-02, PeproTech), 10 ug/ml NT-3 (450-03, PeproTech) and 1 µg/mL Laminin for up to 12 days.

BV2 Culture

BV2 cells were cultured and maintained at 37°C, 95% O_2 and 5% CO_2 in Dulbecco's modified Eagle's medium (31885-023, Gibco) supplemented with 10% (v/v) foetal calf serum (A4768801, ThermoFisher) and 1% pen/strep (15140122, ThermoFisher).

Overexpression of PLCG2 in BV2 cell line

The overexpression construct $PLCγ2^{P522R}$ point mutation was inserted into the human $PLCγ2^{WT}$ plasmid (RC200442, Origene) using Q5® site directed mutagenesis kit (E0554S, NEB) according to manufacturer's protocol. The mutagenesis primers used are listed in supplementary Table 1. For overexpression experiments, in brief BV2 cells were seeded onto either a 12 well plate or 8-well chamber slide (IB-80827, iBIDI) at a density of 140,000 and 21,000 cells per well respectively and allowed to settle for 24 hrs. 2 hrs prior to transfection a complete media change was done with fresh DMEM without pen/strep. For transfection, 50 ηg/100 µl of cDNAs (Control, $PLCG2^{WT}$ and $PLCG2^{P522R}$ plasmid) were mixed with 25 µl/100 µl Opti-MEM→ and 0.27 µl/100 µl of Lipofectamine™ 2000 (ThermoFisher) and incubated for 30 minutes. Afterwards, the media on the cells was replaced with transfection mix and was incubated for 24 hrs. The media was then exchanged for fresh DMEM, and cells were incubated for a further 24 hrs before downstream assays, including uptake and metabolic profiling.

Protein extraction and immunoblotting

Protein was extracted from cultured BV2 cells or 7 day mature iPSC derived microglia by lysis for 30 min at 4^0C in ice cold RIPA buffer (150 mM NaCl, 10 mM Tris, pH 7.2, 0.1% SDS, 1% Triton X-100, 1% deoxycholate, 5 mM EDTA), supplemented with protease (78430, ThermoFisher) and phosphatase inhibitor (524625-1SET, MERCK) cocktails (ThermoFisher). The RIPA soluble fraction was obtained by centrifugation of the samples at 10'000 xg for 10 minutes. Protein concentration was determined using the Pierce BCA Protein Assay Kit (Thermo Fisher Scientific). Samples were mixed with loading buffer (928-40004, Li-Cor) before boiling at 95^0C. SDS-PAGE separation was performed on NuPAGE 4–12% gradient Bis-Tris gels (Thermo Fisher) and proteins were transferred to nitrocellulose membranes (IB23002, ThermoFisher) using an iBLOT2 following manufactures protocol. Membranes were blocked for 1 hour in 3% BSA in TBST (0.1% tween) before incubation with primary antibodies (supplementary Table 2) in 3% BSA in TBST overnight at 4^0C. Membranes were washed 3 times 5 minutes and incubated with secondary antibodies (supplementary Table 2) for 1hr at room temperature before further washes using TBST. Membranes were analysed using a LI-COR Odyssey CLx system and protein levels were quantified using Image Studio Lite (LI-COR Biosciences), normalized to their corresponding β-Actin levels. Statistical significance was assessed using one-way ANOVA.

Phagocytosis assay

For phagocytosis assay 5 x 10^4 iMG progenitors were seeded onto 8-well chamber slide (IB-80827, iBIDI) coated with PDL and matured for 7 days with 50% medium change every other day. Uptake assays were then performed by exchanging 100% media to fresh media supplemented with either 250 nM $A\beta_{1-42}$ HyLite Fluor 647 (AS-60493, AnaSpec), mouse brain purified ^{td}Tomato-tagged synaptosomes generated in-house, FITC-Dextran 4kD (46944, Sigma), FITC-Dextran 150 kD (46946, Sigma), Zymosan beads-568 (Z23374, ThermoFisher) and 75 nM LysoTracker DND-99 (L7528, ThermoFisher) for 100 min. After elapsed time, iMG were washed with PBS and fixed with 4% paraformadehyde for 30 min. Fixed iMG were subsequently stained with SNL (FL-1301-2, Vector) to visualise the membrane and with 2 uM Hoechst (62249, ThermoFisher) nuclear stain. Images were acquired using Nikon A1R inverted confocal microscope (Nikon) running the NIS elements software using 60x oil immersion lens. Acquired images were analysed using FIJI and IMARIS, thresholding to WT/Control, marking ROI and quantified either as %Cell Area or uptake (cargo) volume per total cell volume. Statistical significance was assessed using a Kruskal-Wallis test.

Immunochemiluminiscence Assay (Meso Scale Discovery)

To measure the residual level of Aβ in the co-culture assay, supernatant was collected from co-culture of 21-day mature iPSC derived cortical neurons and 7day mature microglia and centrifuged at 1000G to remove any cellular debris. In brief Immunochemiluminiscence assay was performed by adding 150 µL of Diluent 35 (MSD) to each well of a 96 well multi-spot MSD plate (N45197A-1, MSD) and incubated at

room temperature for 1 hour, on a plate shaker. Subsequently, the plate was washed 3 times with Tris Wash Buffer (MSD). After washing, 25 µL of Aβ detection antibody (6E10, MSD) and 25 µL of prepared samples (cellular supernatant) was added to each well. The plate was incubated at room temperature for 3h, on a plate shaker, prior to washing 4 times with Tris Wash Buffer. 150 µL of 2X Read Buffer (MSD) was added to each well. Samples were analysed on the MSD plate reader using default detection criteria. The MSD read outputs, indicative of Aβ level, were normalized to their corresponding total protein concentration and were analysed using GraphPad. Statistical significance was assessed using a Kruskal-Wallis test.

RT-qPCR analysis

RNA was extracted from iPSC derived microglia (iMG) and/or BV2 using Direct-zol RNA MiniPrep Kit (Zymo research) according to the manufacturer's protocol. For RT-qPCR analysis, RNA was reverse transcribed into cDNA using iScript cDNA synthesis kit (BIO-RAD) according to the manufacturer's protocol. Target specific PCR primers for mouse and human (Supplementary Table 3) were obtained from IDT. For qRT-PCR analysis Takyon Rox SYBR MasterMix dTTP blue (Eurogentec) was used. For relative expression analysis the ΔΔCt comparative method was used to compare TBP normalized expression level of the target mRNA. Data were normalized either to control (BV2) or WT groups (iMG) and are shown as median ± SD. Statistical significance for each gene was assessed using a Kruskal Wallis test.

Cellular respiration assay

To measure oxygen consumption rates (OCR) and extracellular acidification rates (ECAR) in real time, iMG were seeded and matured for 7-days on a Seahorse 96 well cell-culture microplate (PerkinElmer) at a density of 25'000 cells per well. Mature iMG's mitochondrial respiration was then analysed on the seahorse XFe96 Analyser (Agilent Technologies) using a Mitostress test kit (Agilent Technologies) according to manufactures protocol.

For BV2 cells, to measure OCR and ECAR, cells were seeded on a seahorse cell culture plate at a density of 27'000 cells per well and transfected, as described, with cDNA (Control, WT and PLCG2-P522R) constructs. 24 hrs post transfection, real-time mitochondrial respiration was measured using a Mitochondrial stress test kit (Agilent Technologies) on the seahorse XFe96 Analyser. All data were analysed using Wave v2.4.0.6 (Agilent technologies) and Graph pad. Statistica significance was assessed using a Kruskal-Wallis test.

Cell tracking/motility assay

To measure microglia motility, speed, and distance, iMG were plated on a glass bottom Ultra cell carrier 96 well plate (6055302, PerkinElmer), precoated with PDL, and matured for 7 days as previously described. Mature iMG were stained with nuclear mask blue (ThermoFisher) and cell mask orange (ThermoFisher) for 30 min. Cells were then washed with PBS twice and 100 µl of prewarmed microglia media made in FluroBright (A1896701, Gibco) was added. iMGs were imaged for 2 hrs on a high-throughput imaging OperaPhenix (PerkinElmer) with both temp and CO_2 maintained at 37^{o}C and 5%

respectively. Image analysis was done using Harmony cell tracking software. Both tracked nuclear speed and cytoplasmic speed were exported and analysed using Graphpad.

Calcium Imaging

To monitor Ca^{2+} levels in iMG, microglia progenitors were seeded on a glass bottom cell carrier Ultra 96 well plate and glass bottom 8-well chamber ibidi slides, precoated with PDL. iMG were matured for 7 days following the described protocol. To treat cells, mature iMG were washed with PBS once and 100 µl FloBright microglia media supplemented with cell permeable 2 µM Fura Red™, AM, cell permeant (F3021, ThermoFisher) was added to the 96-well plate and 300 µl was added to the iBidi plates and incubated for 30 min. Cells were then washed with PBS and FloBright microglia media devoid of Fura Red was added. Images were taken on a high-throughput microscope OperaPhenix (PerkinElmer) and Nikon spinning disc (Nikon), with analysis being performed using Harmony software and ImageJ. Background was subtracted from each frame and ratio-metric value of bound to unbound Ca^{2+} was extracted and analysed in GrapPad.

Results

PLCγ2 P522R modulates microglia mediated uptake of Aβ and Synaptosomes

To investigate the protective role of PLCγ2^{P522R} in human microglia-like cells, we generated isogenic hiPSCs harbouring the *P522R* polymorph in hetero and homozygosity using CRISPR mediated gene editing, and differentiated them into microglia like cells using a previously described protocol [13]. Upon differentiation, PLCγ2^{WT}, PLCγ2^{HET} and PLCγ2^{HOM} did not display any obvious phenotypic defects and robustly expressed microglia/macrophage associated markers including TMEM119 and IBA1 (SFig 1). Previous data suggests that the PLCγ2-*P522R* variant is a mild hypermorphic gain of function [8] and as expected the PLCγ2^{HET} and PLCγ2^{HOM} variants showed a small but significant increase in PLCγ2 protein levels compared to the PLCγ2^{WT} (Fig. 1A, B).

To understand the role of PLCγ2^{P522R} in two key aspects of neuroAD pathology, we examined whether it affects microglial-mediated Aβ clearance and synaptic pruning. To this end, we incubated PLCγ2^{WT}, PLCγ2^{HET} and PLCγ2^{HOM} iPSC derived microglia with fluorescently tagged $Aβ_{1-42}$ or tDtomato tagged-synaptosomes purified from mouse brain. Microglia expressing the PLCγ2^{P522R} variant demostrated a robust increase in Aβ uptake compared to the control (Fig. 1C, D), irrespective of heterozygosity. We also saw an increase in lysotracker levels, indicating increased acidic endolysosomal vesicles, in PLCγ2 variants compared to the PLCγ2^{WT}, with PLCγ2^{HET} having slightly higher levels than PLCγ2^{HOM} (Fig. 1C, E). By contrast, synaptosome uptake was significantly reduced in PLCγ2^{P522R} variants with a dose dependent reduction between PLCγ2^{HET} and PLCγ2^{HOM} variant cells (Fig. 1F,G). To further establish

whether these findings were associated with the PLCγ2^{P522R} variant, and not a consequence of off-target effects, we transfected BV2 cells, with either a Control, PLCγ2^{WT} or PLCγ2^{P522R} construct, followed by incubation with Aβ_{1-42} peptides and synaptosomes. PLCγ2 expression *per se* resulted in a robust increase in Aβ uptake compared to the control (S. Figure 2) and a non significant mild enhancement (p = 0.3385) was seen in PLCγ2^{P522R} expressing cells. Furthermore, Aβ accumulation was predominately observed in subcellular compartments, such as lysosomes, whilst synaptosomes were internalised by the control, but appeared predominantly bound to the cellular membrane in *P225R* mutants (S. Figure 2). In addition, BV2 cells generally display a small round body with no obvious extensions, similar to the amoeboid-like state reported *in vivo* [14] however, when transfected with PLCγ2 construct these cells displayed a bigger, elongated phenotype with several cytoplasmic extensions, possibly indicating a more ramified state (S. Figure 3).

It has been suggested that Aβ may facilitate synaptic pruning by microglia by acting as a tag for targeting synapses [15]. To investigate whether the hiPSC microglia variants would specifically target Aβ peptides for clearance or indiscriminately target Aβ and synaptosomes, we incubated mature hiPSC derived microglia with Aβ and synaptosomes concurrently. 3D Image analysis showed increased Aβ uptake by PLCγ2 microglia variants compared to controls, with no clear significant difference between the PLCγ2^{HET} and PLCγ2^{HOM} lines (Fig. 2A, B). Synaptosome uptake on the other hand was lower in the PLCγ2^{HET} microglia compared to both PLCγ2^{WT} and PLCγ2^{HOM} cells (Fig. 2A, C), suggesting that the 'dose level' of the *P522R* variant plays a key role in its altered function.

PLCγ2 ^{P522R} affect synaptic pruning in hiPSC derived cortical neuron and microglia co-culture.

The monoculture assays strongly suggests that the PLCγ2^{P522R} protective variant modulates the uptake of Aβ and synaptosomes in an opposing manner. However, this work was conducted in monocultures, which lack the complex neuronal architecture and multicellular networks seen *in vivo*. Hence we replicated our initial experiments in a neuronal-microglial cell co-culture system. PLCγ2^{WT}, PLCγ2^{HET} or PLCγ2^{HOM} microglia progenitor cells were added to 2-week-old iPSC NGN2-derived cortical neurons, bearing the PLCγ2^{HET} polymorph, and kept for a further 7 days in co-culture allowing the microglia to reach maturation. As expected, microglia were actively involved in synaptic pruning, as measured by PSD95 engulfment, in all conditions tested (Fig. 2D-F). However, the PLCγ2^{HET} variant demonstrated significantly reduced uptake of PSD95 compared to the PLCγ2^{WT} variant (Fig. 2D, E). Interestingly, no significant difference was observed with the PLCγ2^{HOM} microglia. This data highlights our finding that the maximal beneficial impact on synapse pruning is seen in cells heterozygous for the variant. The disparity between our mono- and co-culture findings further suggests that additional mechanisms involved in synaptic pruning beyond phagocytic uptake *per se* may be subtly impacted by the presence of PLCγ2^{P522R}. We also collected supernatant from the co-culture assay to probe for Aβ_{1-40} levels (released endogenously by the iPSC derived neurons) using an MSD plate reader. While all conditions containing microglia recorded reduced Aβ level compared to neuronal cells in the absence of microglia, only cultures

containing microglia heterozygous for the PLCγ2^{P522R} variant reached significance (p = 0.0109), indicative of increased Aβ uptake by these cells (Fig. 2F). These results collectively establish that heterozygous PLCγ2^{P522R} expression enhances the clearance and modulation of Aβ peptides while sparing synapses in a co-culture setup, providing a possible mechanism for AD protection.

PLCγ2 P522R differential selectivity is driven by cargo size.

PLCγ2^{P522R} has previously been reported to influence selective cargo uptake, suggesting a shift towards endocytic pathways [12]. Given the differential impact of heterozygous and homozygous PLCγ2^{P522R} on Aβ and synaptosome uptake, we sought to further investigate whether similar cargo selectivity differences were observed in our microglial cell model. We assessed hiPSC derived microglial uptake of Zymosan beads of approximately 3 μm diameter and two dextran glucans of 150 kD and 4 kD. Consistent with our findings for Aβ, PLCγ2^{HET} microglia had a significantly higher uptake of Dextran^{4kD} and Dextran^{150kD} compared to the PLCγ2^{WT} and PLCγ2^{HOM} variants (Fig. 3A-D). Likewise, both PLCγ2^{HET} and PLCγ2^{HOM} cells showed a reduced uptake of zymosan particles compared to PLCγ2^{WT} microglia (Fig. 3E, F), consistent with the previously reported shift towards the endocytic uptake of smaller cargoes.

Similar studies in BV2 cells over expressing either WT or *P522R* PLCγ2 showed that over expression of the protein, irrespective of the variant, resulted in a marked increase in zymosan uptake, and reduced uptake of both the dextran substrates, supporting the notion that PLCγ2 plays a key role in the regulation of microglial uptake size-selectivity. For both zymosan and 4kDa Dextran, the *P552R* variant displayed a trend towards reduced effects compared to WT over expression, in contrast, the *P522R* variant significantly enhanced uptake of Dextran^{150kD} (S. Figure 4).

PLCγ2 P522R modulates multiple functions of hiPSC derived microglia.

To begin to unpick the cellular pathways that may play a role in PLCγ2^{P522R} altered uptake of AD relevant cargoes, we investigated the effect of the variant on the expression profiles of a number of functionally relevant microglial genes. We focused on pathways previously identified as potentially playing a role in AD progression, as well as core genes involved in modulating microglial immune function and functional status.

We harvested 7 day differentiated hiPSC derived microglia in the absence of additional stimulus (‘resting’) and probed the expression profile of a selection of different genes (Fig. 4). We saw significant increases in the expression of a small number of genes associated with lipid metabolism (LIPA; p = 0.0374, APOE; p = 0,0331, PLIN2; p = 0.0422), endosome/phagosome maturation (RAB5; p = 0.0351, RAB7; p = 0.0174) and cytokines/chemokines (IL-10; p = 0.0043, CX3CR1; p = 0.0475) in PLCγ2^{HET} cells compared to PLCγ2^{WT} cells. Only one of these genes, APOE, was found to be significantly increased in PLCγ2^{HOM} cells (p = 0.0374). A small number of additional genes also showed a trend towards increased expression in PLCγ2^{HET} cells, although these did not reach significance (CD68; p = 0.1656, P2RY12; p = 0.1739, NLRP3; p = 0.1498, CYP1A1; p = 0.1209, CYP1B1; p = 0.1219, TMEM119; p = 0.1739). These

findings suggest that PLCγ2^{HET} cells display a subtly different expression profile to both control and PLCγ2^{HOM} cells even in a resting state, that may underpin the protective effects of the *P522R* variant seen in our functional assays and in AD.

Plcγ2 P522r Enhances Mitochondrial Oxidative Phosphorylation In Hipsc Derived Microglia

The bioenergetic profile of microglia is directly linked to their functional state. Given that the PLCγ2^{P522R} variant impacts on metabolic and mitochondrial biogenesis pathways and shows increased Aβ uptake, an energy demanding process, we speculated that it may impact directly on mitochondrial function. To investigate the role of PLCγ2 on mitochondrial respiration we employed an Agilent Seahorse assay to look at the mitochondrial oxygen consumption rate (OCR), a measure of mitochondrial function. Under a mitochondrial stress test paradigm, PLCγ2^{HET} and PLCγ2^{HOM} cells showed a dose-dependent increase in basal and maximal respiration compared to PLCγ2^{WT} cells (Fig. 5A-C). ATP production was also increased (Fig. 5D). Proton leak (the migration of protons across the mitochondrial membrane independent of ATP-synthase) was dose dependently higher in the PLCγ2^{P522R} cells compared to the PLCγ2^{WT} variant (Fig. 5E). It has been suggested that increased proton leak is directly related to the prevention of oxidative stress, the inhibition of fatty acid induced mitochondrial damage and the control of oxidative phosphorylation [16], potentially protecting the cell from excessive damage. Hence, our findings suggest superior mitochondrial performance in PLCγ2^{P522R} variants.

To check whether increased mitochondrial function was simply a result of increased mitochondrial number we incubated matured microglia with mitotracker. Confocal imaging revealed a comparable level of mitotracker in all PLCγ2 variant cells, thus mitochondrial number is unliely to be affected by the presence of the *P522R* variant (Fig. 5F, G). We also probed for TOMM20 (Translocase Of Outer Mitochondrial Membrane 20); part of the mitochondrial receptor complex responsible for the recognition and translocation of cytosolically synthesized mitochondrial preproteins. Western blot analysis revealed no difference in TOMM20 protein expression between PLCγ2^{P522R} and PLCγ2^{WT} cells (Fig. 5H, I). These data suggest that altered mitochondrial function was solely responsible for enhanced OCR and ATP production as opposed to changes in mitochondrial number.

To validate our hiPSC derived microglia findings we again transfected BV2 cells with the WT or *P522R* variant PLCγ2, or control constructs and monitored OCR in real time using the seahorse extracellular flux analyser. Consistent with our hiPSC derived cells, BV2 cells overexpressing PLCγ2^{P522R} and PLCγ2^{WT} had significantly higher levels of basal respiration, maximal respiration and ATP production compared to those transfected with the control construct (SFig 5). Interestingly, while maximal respiration in cells over expressing PLCγ2^{P522R} was significantly lower than cells over expressing the WT protein, the ATP production was comparable, indicating an optimal level of mitochondrial function in PLCγ2^{P522R} cells that efficiently met the ATP demand (SFig 5C, D). Likewise, BV2 cells with PLCγ2 overexpression showed

a higher level of proton leak compared to controls, with no clear difference between PLCγ2^{WT} and PLCγ2^{P522R} (SFig 5E). In conclusion, we identified a novel role of PLCγ2 on mitochondrial function, which indicates better microglial metabolic fitness.

Microglia With Plcγ2 P522r Variant Have Higher Ca Signalling And Increased Motility

PLCγ2 activity can induce calcium influx from the ER through the binding of IP3 to its receptor in the ER, IP3R [17]. This massive cytoplasmic Ca^{2+} influx is critical for various downstream signalling pathways that modulate numerous microglial functions. Hence, to investigate whether there are any differences in Ca^{2+} levels between the different PLCγ2 variants we incubated the hiPSC derived microglia with the cell permeable, light-excitable calcium sensor molecule Fura Red™. Live-cell imaging revealed significantly higher Ca^{2+} intensities, indicating higher Ca^{2+} levels, in PLCγ2^{HET} microglia compared to PLCγ2^{WT} cells, that was not seen in PLCγ2^{HOM} cells (Fig. 6A, B). Indeed, PLCγ2^{HOM} microglia had slightly reduced Ca^{2+} levels compared to PLCγ2^{WT} cells, although this did not reach significance ($p = 0.1528$). We also assessed changes in resting Ca^{2+} levels over time. Microglia were treated with Fura Red™ for 30 min and Ca^{2+} intensity monitored for 120 min. Consistent with our previous findings, both PLCγ2^{HET} and PLCγ2^{WT} microglia variants had persistently higher basal Ca^{2+} intensity compared to microglia with the PLCγ2^{HOM} variant (SFig 6).

The role of Ca^{2+} in cell migration and adhesion is well-documented, hence given the differences in Ca^{2+} intensity among our PLCγ2 variants, we decided to investigate if this may impact on microglial motility. We assessed two parameters: nuclear tracking, for whole cell migration, and cytoplasmic tracking, for microglial ramification and surveillance. Microglia were tracked for two hours and their motility assessed in untreated (homeostatic) conditions. Consistent with the changes observed in Ca^{2+} levels, PLCγ2^{HET} microglia had significantly higher nuclear speeds compared to PLCγ2^{WT} ($p = 00002$) and PLCγ2^{HOM} ($p = 0.0001$) variants, which themselves did not significantly differ ($p = 0.3219$) (Fig. 6C). Cytoplasmic motility was also significantly enhanced in PLCγ2^{HET} cells, potentially indicative of increased surveillance activity (Fig. 6D).

In addition, by measuring total distance covered by the cells, we investigated whether the tracked speed had any connection to distance travelled. Consistent with our tracked speed findings, PLCγ2^{HET} significantly outperformed both PLCγ2^{WT} and PLCγ2^{HOM} variants in total distance covered (Fig. 6E). Our findings indicate that PLCγ2^{HET} microglia were more active in both surveillance and migration compared to PLCγ2^{WT} and PLCγ2^{HOM} microglia, and this could be tied to their housekeeping Ca^{2+} level.

Discussion

In this study, we investigated the impact of the AD protective PLCγ2^{P522R} variant on muman microglial cell functions. We used CRISPR editing to generate PLCγ2^{HET} and PLCγ2^{HOM} hiPSC cells, and differentiated them into microglia that exhibit functional and transcriptional profiles consistent with human microglia [13]. We were able to show that the presence of the *P522R* variant resulted in increases in PLCγ2 levels, as previously reported [8]. It also increased microglial uptake of the Aβ peptide, accompanied by a reduction in synapse pruning, two key pathological processes in AD. We provide evidence that this discrimination appears to be primarily driven by cargo size, and that cells expressing the PLCγ2^{P522R} variant have enhanced mitochondrial function and cell motility, potentially associated with increased intracellular Ca^{2+}. We have also identified transcriptional changes in a number of genes associated with lipid metabolism, endosome/phagosome maturation and immune function in resting state PLCγ2^{HET} microglia, which highlight potential pathways that may underpin the protective capacity of the PLCγ2^{P522R} variant in AD. Crucially, we have shown that the impact of PLCγ2^{P522R} is dependent on dose, with heterozygous cells overall showing a more beneficial profile than homozygous cells.

The clearance of Aβ, along with other cellular debris, is an important feature of microglial phagocytic function in AD. Several other polymorphisms implicated as risk factors in AD, such as the R47H TREM2 mutation, result in alterations to microglial phagocytic capacity that lead to reduced clearance of Aβ aggregates and neuronal decline [18, 19]. In our hiPSC derived microglia assay, PLCγ2^{P522R} enhanced the uptake of Aβ compared to PLCγ2^{WT} microglia, suggesting that the variant may positively impact directly on disease relevant pathology clearance, as previously suggested [12]. Consistent with this increased Aβ clearance, lysotracker levels, which indicate acidic vesicles such as lysosomes, were higher in both PLCγ2^{HET} and PLCγ2^{HOM} microglia variants compared to PLCγ2^{WT} cells. Interestingly, PLCγ2^{HET} microglia showed a more robust increase in lysotracker levels than PLCγ2^{HOM} cells, suggesting that there may be a narrow functional level (“sweet spot”) of PLCγ2^{P522R} that leads to improved outcomes. This is supported by the fact that while a number of the processes we assessed did appear to be ‘dose dependently’ modified by heterozygous vs. homozygous expression of the PLCγ2^{P522R} variant, other processes were preferentially impacted only in heterozygous cells. Indeed, a number of gain of function mutations in PLCγ2 have been linked to immune disorders, including PLAID (PLCγ2-associated antibody deficiency and immune dysregulation syndrome), APLAID (autoinflammation, antibody deficiency and immune dysregulation syndrome) and FCAS3 (familial cold autoinflammatory syndrome), as well as a subset of CVID (common variable immunodeficiency) patients [20–27]. These clearly indicate that a significant gain of function of PLCγ2 can lead to deleterious impacts on the immune system.

In the central nervous system, microglia shape neuronal synaptic connections and strength during development, through the removal of excess synapses [28]. While microglia mediated synaptic pruning is a fundamental physiological process during development, its proposed reactivation during aging has deleterious consequences and may account for much of the memory loss and cognitive decline observed in AD [15]. It has recently been reported that individuals with MCI (mild cognitive impairment), who carry the PLCγ2^{P522R} variant had better cognitive performance even in the presence of the APOE4 AD risk gene

[29]. Here we show hiPSC microglia with the PLCγ2^{P522R} variant had decreased synaptosome uptake compared to WT cells. Moreover, we were able to demonstrate that these PLCγ2^{P522R} microglia selectively spare synaptosomes while maintaining efficient clearance of Aβ when treated concurrently with both biological cargoes. These finding were replicated in BV2 cells over expressing exogenous human PLCγ2^{WT} or PLCγ2^{P522R}, indicating a possible connection between increased expression of PLCγ2 and reduced synapse uptake. We provide further evidence of this in our neuronal and microglial co-culture study, where we saw a reduction in synaptic pruning by PLCγ2^{P522R} microglia, as evidenced by reduced levels of PSD95 within microglial cells. Interestingly, this was once again more robustly observed in PLCγ2^{HET} cells, supporting the notion of a 'sweet spot' for maximal beneficial impacts on microglial function.

The most prevailing question is how does the PLCγ2^{P522R} variant modulate diverse microglial functions to protect a degenerating brain? Our gene expression study highlights a number of different functional pathways that appear to be activated in PLCγ2^{HET} microglia, notably those relating to lipid metabolism, endosome/phagosome maturation and immune function. Proinflammatory environments and signalling are a prominent observation in AD brain pathology [30]. Our findings suggest a significant increase in the expression of the anti-inflammatory cytokine, interleukin-10 (IL-10), which is known to inhibit the synthesis of pro-inflammatory cytokines, and may promote the differentiation of microglia into the anti-inflammatory state, classically known as M2 or homeostatic state [31]. Interestingly, IL-10 deficiency has also been shown to exacerbate Tau pathology [32]. This, combined with our data, provides a potential route whereby the PLCγ2^{P522R} variant may impact at least in part on both primary pathologies associated with AD to reduce disease risk.

We also report significant increases in the expression of the chemokine receptor, CX3CR1 in PLCG2^{HET} cells. Within the CNS, this receptor is expressed exclusively by microglia, and binds to the neuronally expressed chemokine, CX3CL1 (fractalkine). The exact function of this interaction is not yet clear, but evidence suggests it plays an important role in the regulation of synaptic function, with CX3CR1 deficiency resulting in cognitive and LTP impairments indicative of altered synaptic plasticity [33, 34]. Certainly increased expression of CX3CR1 attenuates microglial inflammatory responses to LPS (liposccharide) (Inoue et al., 2021, PLOS One), while deletion results in an increased inflammatory response and phagocytic acivity (Murai et al, 2020, Eur J Neurosci). It is therefore possible that the increase in CX3CR1 we observe in resting state PLCγ2^{HET} microglia is linked to the reduction in synapse phagocytosis seen in these cells, although more work is required to unpick the mechanism that may underpin this.

A growing body of evidence suggests that lipid metabolism is crucial to fuel microglial functions such as phagocytosis, and can vary depending upon the activation status of the cell (reviewd in [35]). Previous studies have shown that PLCG2 acts downstream of TREM2, and knock out of either protein results in lipid accumulation deficits and a failure to activate key lipid processing genes such as LIPA and APOC1 [11], as well as a generalised alteration in the overall lipidome of the cells. In the current study,

heterozygous PLCγ2^{P522R} induced increases in the expression of genes associated with phagocyte maturation (RAB5, RAB7) and various aspects of lipid metabolism (LIPA, APOE, PLIN2) in resting state microglia, an effect which is not seen in homozygous cells. This may suggest that these heterozygous cells are 'primed' to more readily respond to an inflammatory challenge, and can therefore more efficiently uptake and phagocytose targets such as Aβ when required.

It is important to acknowledge that the gene expression changes we observed in the PLCγ2^{HET} microglia were all seen in resting state cells, without LPS or other disease relevant immune challenge. These expression changes are likely to be important factors in the protective capacity of PLCγ2^{P522R}. LOAD develops over many years, rather than arising as a result of a single acute challenge, thus these low level ongoing changes likely reflect the chronic impact of the variant on general microglial function. However, it is probable that additional changes will be observed in response to immune challenge, and further work is required to eludicate these changes, and understand how they impact on microglial function, to improve target cargo uptake and preserve synapses. Indeed, we identified a number of additional genes that trended towards a difference between PLCγ2^{HET} and PLCγ2^{WT} cells, that may indicate a subset of genes 'primed' to respond to immune challenge. Loss of PLCG2 results in a spectrum of gene expression changes in microglia both at rest, and in response to TLR stimulation [11], and intriguingly, this TLR induced profile appears distinctly different from that seen with TREM2 knockout, suggesting that PLCG2 may interact independently with both TREM2 and TLR linked pathways, although we did not see significant changes in the basal expression of TREM2 or TLR4, or functionally associated proteins such as NLRP3 in our cells. A broad spectrum of genes expression changes have also been reported in homozygous PLCγ2^{P522R} knock-in mice [36]. However, given our findings, which suggest that heterozgosity is important for maximimal benefits from the variant, examining the difference between heterozygous and homozygous PLCγ2^{P522R} basal and stimulated gene expression profiles may be invaluable in more clearly identifying specific functional changes responsible for the protective impact of PLCγ2^{P522R} in LOAD.

The highly dynamic nature of microglia makes them heavily dependent on efficient energy expenditure to meet basic housekeeping demands. To maintain brain homeostasis and surveillance, microglia require energy-demanding cytoskeleton remodelling, necessary for extending and retracting their ramified processes, to constantly scan their surroundings [37, 38]. Whilst in a resting state, microglia use mitochondrial respiration, specifically OXPHOS (oxidative phosphorylation) as their main source of energy, although resting state is a misconception, since microglia are never quiescent, rather they are constantly engaged in parenchymal surveillance [38]. Our findings indicate that microglia expressing PLCγ2^{P522R} in general show enhanced mitochondrial respiration as well as significantly higher ATP production, which was not associated with increases in mitochondrial number but rather changes in mitochondrial function.

Mitochondrial function directly correlates with cytoplasmic Ca^{2+} levels, which could underlie the enhancement we observed in the PLCγ2^{P522R} cells. PLCγ2 is a direct modulator of Ca^{2+} influx from the

endoplasmic reticulum (ER) via its hydrolysis of PIP2, leading to the production of IP3, which then interacts with its receptor IP3R1 [39]. Recent reports have demonstrated that the presence of the PLCγ2^{P522R} variant in microglia enhances Ca^{2+} release in response to physiological stimuli [12]. In our study, we found that PLCγ2^{HET} microglia showed higher levels of basal intracellular Ca^{2+} than PLCγ2^{WT} cells in the absence of any stimulus, supporting the notion that the PLCγ2^{HET} cells may be 'primed' to respond more rapidly to an inflammatory challenge. This increase was not observed in the PLCγ2^{HOM} cells, once again highlighting the delicate balance of P522R dose on PLCγ2 function. Interestingly, PLCγ2^{HOM} cells did demonstrate a greater enhancement of mitochondrial function than the PLCγ2^{HET} cells, in the absence of any change in Ca^{2+} levels. This separation between Ca^{2+} levels and mitochondrial performance suggests that other as yet unidentified factors may play a key role in modulating microglial cell energy homeostasis.

Ca^{2+} currents have also been implicated in the regulation of microglial motility (reviewed in [40]. Consistent with the increase we see in intracellular Ca^{2+} in PLCγ2^{HET} cells, they also demonstrated enhanced mobility compared to PLCγ2^{WT} cells. Both whole cell movement, detected via nuclear tracking, as well as surveillance, detected via assessing cytoplasmic movement alone, were enhanced. PLCγ2^{HOM} cells also showed increased surveillance, but their nuclear movement did not differ from PLCγ2^{WT} cells, once again highlighting the delicate functional balance between heterozygous and homozygous expression of the P522R variant.

Our study is the first to suggest that the protective nature of the PLCγ2^{P522R} variant in AD may reflect a selective increase in microglial clearance of Aβ, coupled with a preservation of synpases. This is accompanied by an increase in mitochondrial fitness and microglial motility, suggesting that PLCγ2^{P522R} may enhance basal microglial functioning, leading to a relative protection against the accumulation of pathogenic proteins seen in both healthy aging and AD. A number of resting state transcriptional changes are associated with this altered function, which appears to be critically dependent on PLCγ2^{P522R} 'dose', with heterozygous expression of the variant optimal.

Conclusions

This data highlights the complex role of microglia in health and disease, and the importance of understanding how risk factors such as PLCγ2^{P522R} exert their effects, and how protein or variant dose can play a key role in modifying cellular functions. It suggests that more investigation is needed into the delicate balance of PLCG2 and microglial function in health and disease, and shows the need for caution and rigorous testing when targeting these pathways for therapeutic development.

Abbreviations

Ab
amyloid beta

ABCA1
ATP Binding Cassette Subfamily A Member 1
ABCA7
ATP Binding Cassette Subfamily A Member 7
ABI3
ABI family member 3
AD
Alzheimer’s disease
AHR
Aryl Hydrocarbon Receptor
AHRR
Aryl-Hydrocarbon Receptor Repressor
AiF1
Allograft Inflammatory Factor 1
APLAID
autoinflammation, antibody deficiency and immune dysregulation syndrome
APOE
Apolipoprotein E
ARNT
Aryl Hydrocarbon Receptor Nuclear Translocator
ATP
Adenosine 5” Triphosphate
B2M
Beta-2-Microglobulin
C1QA
Complement C1q subcomponent subunit A
CD14
Cluster of Differentiation 14
CD33
Cluster of Differentiation 33
CD52
Cluster of Differentiation 52
CD68
Cluster of Differentiation 68
CD9
Cluster of Differentiation 9
CLCN7
Chloride Voltage-Gated Channel 7
CNS
central nervous system

CSF1
Colony Stimulating Factor 1
CST3
Cystatin 3
CTSB
Cathepsin B
CTSD
Cathepsin D
CVID
common variable immunodeficiency
CX3CR1
C-X3-C Motif Chemokine Receptor 1
CYP1A1
Cytochrome P450 Family 1 Subfamily A Member 1
CYP1B1
Cytochrome P450 Family 1 Subfamily B Member 1
DAM
disease associated microglia
ER
endoplasmic reticulum
FABP5
Fatty Acid Binding Protein 5
FCAS3
familial cold autoinflammatory syndrome
HEXB
Hexosaminidase Subunit Beta
hiPSC
human induced pluripotent stem cell
HK3
Hexokinase 3
IBA1
Ionized calcium binding adaptor molecule 1
IFNG
Interferon Gamma
IL10
Interleukin 10
IL1B
Interleukin 1 Beta
IL4
Interleukin 4

IL6
Interleukin 6
IP3R
Inositol Trisphosphate receptor
LAMP1
Lysosomal Associated Membrane Protein 1
LAMP2
Lysosomal Associated Membrane Protein 1
LIPA
Lipase A, Lysosomal acid type
LOAD
late onset Alzheimer's disease
MCI
mild cognitive impairment
NFKB
Nuclear Factor Kappa B Subunit
NLRP3
NLR Family Pyrin Domain Containing 3
OCR
oxygen consumption rate
P2RY12
Purinergic Receptor P2Y12
PFKFB1
6-phosphofructo-2- kinase/fructose-2,6-biphosphatase 1
PFKFB3
6-phosphofructo-2- kinase/fructose-2,6-biphosphatase 3
PLAID
PLCγ2-associated antibody deficiency and immune dysregulation syndrome
PLCG2/PLCg2
Phospholipase C Gamma 2
PLIN2
Perilipin 2
PSD95
postsynaptic density protein 95
RAB5
Member RAS Oncogene Family5
RAB7
Member RAS Oncogene Family7
SIRPa
Signal regulatory proteinα

SPI1
Spi-1 proto-oncogene
TFB2M
Transcription factor B2, Mitochondrial
TLR4
Toll Like Receptor 4
TMEM119
Transmembrane Protein 119
TOMM20
Translocase Of Outer Mitochondrial Membrane 20
TREM2
Triggering Receptor Expressed on Myeloid Cells 2
TSPO
Translocator protein
TYROBP
Protein Tyrosine Kinase-Binding Protein
WT
wild type

Declarations

Ethics approval and consent to participate

Not applicable

Consent for publication

Not applicable

Availability of data and materials

All data generated or analysed during this study are included in this published article [and its supplementary information files]

Competing interests

The authors declare that they have no competing interests

Funding

This work was supported by the Van Geest Foundtation, and the UK Dementia Research Institute which receives its funding from UK DRI Ltd, funded by the UK Medical Research Council, Alzheimer's Society and Alzheimer's Research UK.

Authors' contributions

SS and JCM designed experiments, analysed data and wrote the manuscript. SS, NKS, IC, and MM performed experiments. GC developed and wrote the cell tracking script. SS, ACV and JCM interpreted data, ACV and MDR advised on experimental design. All authors edited the manuscript.

Acknowledgements

We would like to acknowledge Mr Tomas Solomon, who helped produce the graphical abstract generated for this manuscript.

References

1. Heneka MT, et al. *Neuroinflammation in Alzheimer's disease*, in *The Lancet Neurology*. Elsevier; 2015. pp. 388–405.
2. Ginhoux F, et al. Fate Mapping Analysis Reveals That Adult Microglia Derive from Primitive Macrophages. 330. New York: Science; 2010. p. 841.
3. Nayak D, Roth TL, McGavern DB. *Microglia Development and Function*, in Annual Review of Immunology. 2014. p. 367–402.
4. Ling EA, et al. *Microglia: its development and role as a neuropathology sensor*, in *Progress in Brain Research*. Elsevier; 2001. pp. 61–79.
5. Perry VH. The influence of systemic inflammation on inflammation in the brain: implications for chronic neurodegenerative disease. In: Brain, Behavior, and Immunity. Academic Press; 2004. pp. 407–13.
6. Keren-Shaul H, et al., *A Unique Microglia Type Associated with Restricting Development of Alzheimer's Disease*, in *Cell*. 2017, Cell Press. p. 1276–1290.e17.
7. Sims R, et al., *Rare coding variants in PLCG2, ABI3 and TREM2 implicate microglial-mediated innate immunity in Alzheimer's disease*, in *Nature genetics*. 2017, NIH Public Access. p. 1373.
8. Magno L, et al. Alzheimer's disease phospholipase C-gamma-2 (PLCG2) protective variant is a functional hypermorph. Alzheimers Res Ther. 2019;11(1):16.
9. Rhee SG. Regulation of phosphoinositide-specific phospholipase C. In: Annual review of biochemistry. National Center for Biotechnology Information (US); 2001. pp. 281–312.
10. Patterson RL, et al. Phospholipase C-γ Is Required for Agonist-Induced Ca2 + Entry. In: Cell. Elsevier; 2002. pp. 529–41.
11. Andreone BJ, et al., *Alzheimer's-associated PLCγ2 is a signaling node required for both TREM2 function and the inflammatory response in human microglia*, in *Nature Neuroscience 2020*. 2020. p. 1–12.
12. Maguire E, et al. PIP2 depletion and altered endocytosis caused by expression of Alzheimer's disease-protective variant PLCgamma2 R522. EMBO J. 2021;40(17):e105603.

13. Haenseler W, et al., *A Highly Efficient Human Pluripotent Stem Cell Microglia Model Displays a Neuronal-Co-culture-Specific Expression Profile and Inflammatory Response*, in *Stem Cell Reports*. 2017, Cell Press. p. 1727–1742.
14. Cai Z, Hussain MD, Yan LJ. Microglia, neuroinflammation, and beta-amyloid protein in Alzheimer's disease. Int J Neurosci. 2014;124(5):307–21.
15. Rajendran L, Paolicelli RC, *Microglia-Mediated Synapse Loss in Alzheimer's Disease*. 2018.
16. Cheng J, et al. *Mitochondrial proton leak plays a critical role in pathogenesis of cardiovascular diseases*, in *Advances in Experimental Medicine and Biology*. New York: Springer; 2017. pp. 359–70.
17. Kadamur G, Ross EM, *Mammalian Phospholipase C*. 2013.
18. Arcuri C, et al., *The Pathophysiological Role of Microglia in Dynamic Surveillance, Phagocytosis and Structural Remodeling of the Developing CNS*, in Frontiers in Molecular Neuroscience. 2017.
19. Zhao Y, et al., *TREM2 Is a Receptor for β-Amyloid that Mediates Microglial Function*, in *Neuron*. 2018, Cell Press. p. 1023–1031.e7.
20. Novice T, et al. A Germline Mutation in the C2 Domain of PLCgamma2 Associated with Gain-of-Function Expands the Phenotype for PLCG2-Related Diseases. J Clin Immunol. 2020;40(2):267–76.
21. Kutukculer N, et al. Four diseases, PLAID, APLAID, FCAS3 and CVID and one gene (PHOSPHOLIPASE C, GAMMA-2; PLCG2): Striking clinical phenotypic overlap and difference. Clin Case Rep. 2021;9(4):2023–31.
22. Ombrello MJ, et al., *Cold urticaria, immunodeficiency, and autoimmunity related to PLCG2 deletions.*, in *The New England journal of medicine*. 2012, NIH Public Access. p. 330-8.
23. Zhou Q, et al. A hypermorphic missense mutation in PLCG2, encoding phospholipase Cgamma2, causes a dominantly inherited autoinflammatory disease with immunodeficiency. Am J Hum Genet. 2012;91(4):713–20.
24. Neves JF, et al. Novel PLCG2 Mutation in a Patient With APLAID and Cutis Laxa. Front Immunol. 2018;9:2863.
25. Deza G, et al. Acquired Cold Urticaria vs. Autoinflammatory Diseases, Genetic and Clinical Profile and Differential Diagnosis: Study of a Cohort of Patients in a Tertiary Reference Centre. Acta Derm Venereol. 2019;99(12):1071–7.
26. Bogaert DJ, et al. Genes associated with common variable immunodeficiency: one diagnosis to rule them all? J Med Genet. 2016;53(9):575–90.
27. Chae JJ, et al., *Connecting two pathways through Ca 2 + signaling: NLRP3 inflammasome activation induced by a hypermorphic PLCG2 mutation.*, in *Arthritis & rheumatology (Hoboken, N.J.)*. 2015, NIH Public Access. p. 563-7.
28. Paolicelli RC, et al., *Synaptic pruning by microglia is necessary for normal brain development*, in *Science*. 2011, American Association for the Advancement of Science. p. 1456–1458.
29. Kleineidam L, et al., *PLCG2 protective variant p.P522R modulates tau pathology and disease progression in patients with mild cognitive impairment*. 2020. p. 1025–1044.

30. Heneka MT, et al., *NLRP3 is activated in Alzheimer's disease and contributes to pathology in APP/PS1 mice*, in *Nature*. 2013, NIH Public Access. p. 674–678.
31. Laffer B, et al. Loss of IL-10 Promotes Differentiation of Microglia to a M1 Phenotype. Front Cell Neurosci. 2019;13:430.
32. Weston LL, et al. Interleukin-10 deficiency exacerbates inflammation-induced tau pathology. J Neuroinflammation. 2021;18(1):161.
33. Rogers JT, et al. CX3CR1 deficiency leads to impairment of hippocampal cognitive function and synaptic plasticity. J Neurosci. 2011;31(45):16241–50.
34. Maggi L, et al. CX(3)CR1 deficiency alters hippocampal-dependent plasticity phenomena blunting the effects of enriched environment. Front Cell Neurosci. 2011;5:22.
35. Yang S, et al. Microglia reprogram metabolic profiles for phenotype and function changes in central nervous system. Neurobiol Dis. 2021;152:105290.
36. Takalo M, et al. The Alzheimer's disease-associated protective Plcgamma2-P522R variant promotes immune functions. Mol Neurodegener. 2020;15(1):52.
37. Davalos D, et al., *ATP mediates rapid microglial response to local brain injury in vivo*, in *Nature Neuroscience*. 2005, Nature Publishing Group. p. 752–758.
38. Nimmerjahn A, Kirchhoff F, Helmchen F, *Neuroscience: Resting microglial cells are highly dynamic surveillants of brain parenchyma in vivo*, in *Science*. 2005, American Association for the Advancement of Science. p. 1314–1318.
39. Bunney TD, Katan M. *PLC regulation: Emerging pictures for molecular mechanisms*, in *Trends in Biochemical Sciences*. Elsevier Ltd; 2011. pp. 88–96.
40. Umpierre AD, Wu LJ. How microglia sense and regulate neuronal activity. Glia. 2021;69(7):1637–53.

Figures

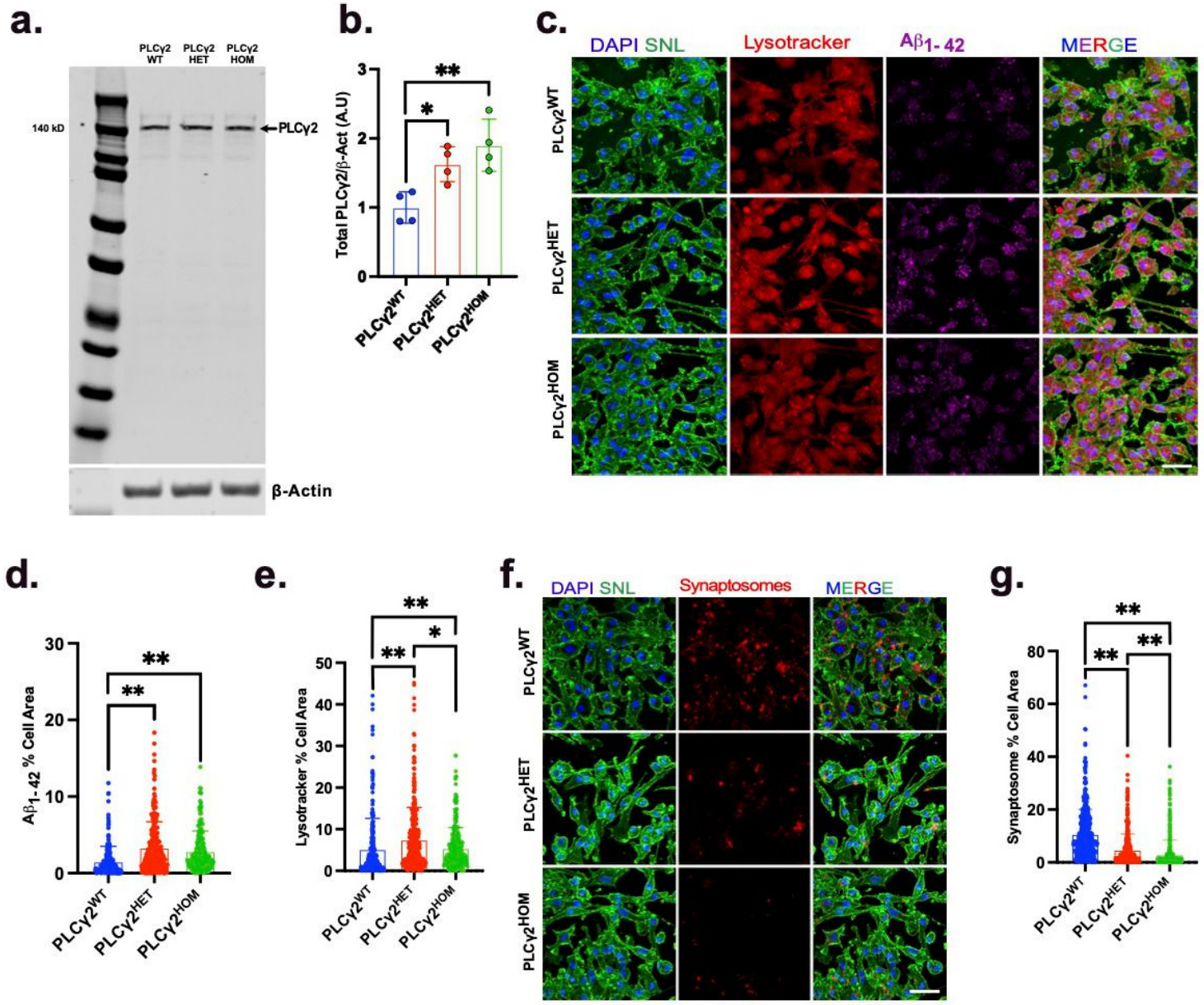

Figure 1

PLCg2^{P522R} enhances Ab uptake while reducing synaptosome uptake.

a-b, Western blot analysis of total PLCg2 protein level in PLCg2 wild type (PLCg2^{WT}), heterozygous (PLCg2^{HET}), and homozygous (PLCg2^{HOM}) hiPSC-derived microglia cells. Expression levels were normalised to b-actin. Data is presented as mean ± SD and analysed using one-way ANOVA with the Tukey multiple comparisons test. (b) **c-e,** Fluorescent confocal analysis of Ab_{1-42} HyLite Fluor 647 uptake (magenta) and lysotracker levels (red) in PLCg2^{WT}, PLCg2^{HET} and PLCg2^{HOM} hiPSC derived microglia cells. Internalised Ab (d) and lysosome (e) levels are expressed as a proportion of total cell area, detected using SNL stain (green). **f-g,** Fluorescent confocal analysis of tdTomato-synaptosome uptake (red) in PLCg2^{WT}, PLCg2^{HET} and PLCg2^{HOM} hiPSC derived microglia cells. Internalised synaptosome levels are expressed as a proportion of total cell area, detected using SNL stain (green). Data is presented as mean

± SD and unless otherwise described was analysed using the Kruskal-Wallis with Dunns multiple comparisons test. (*p<0.05, **p<0.01, n=3-9, Scale bar 50mM).

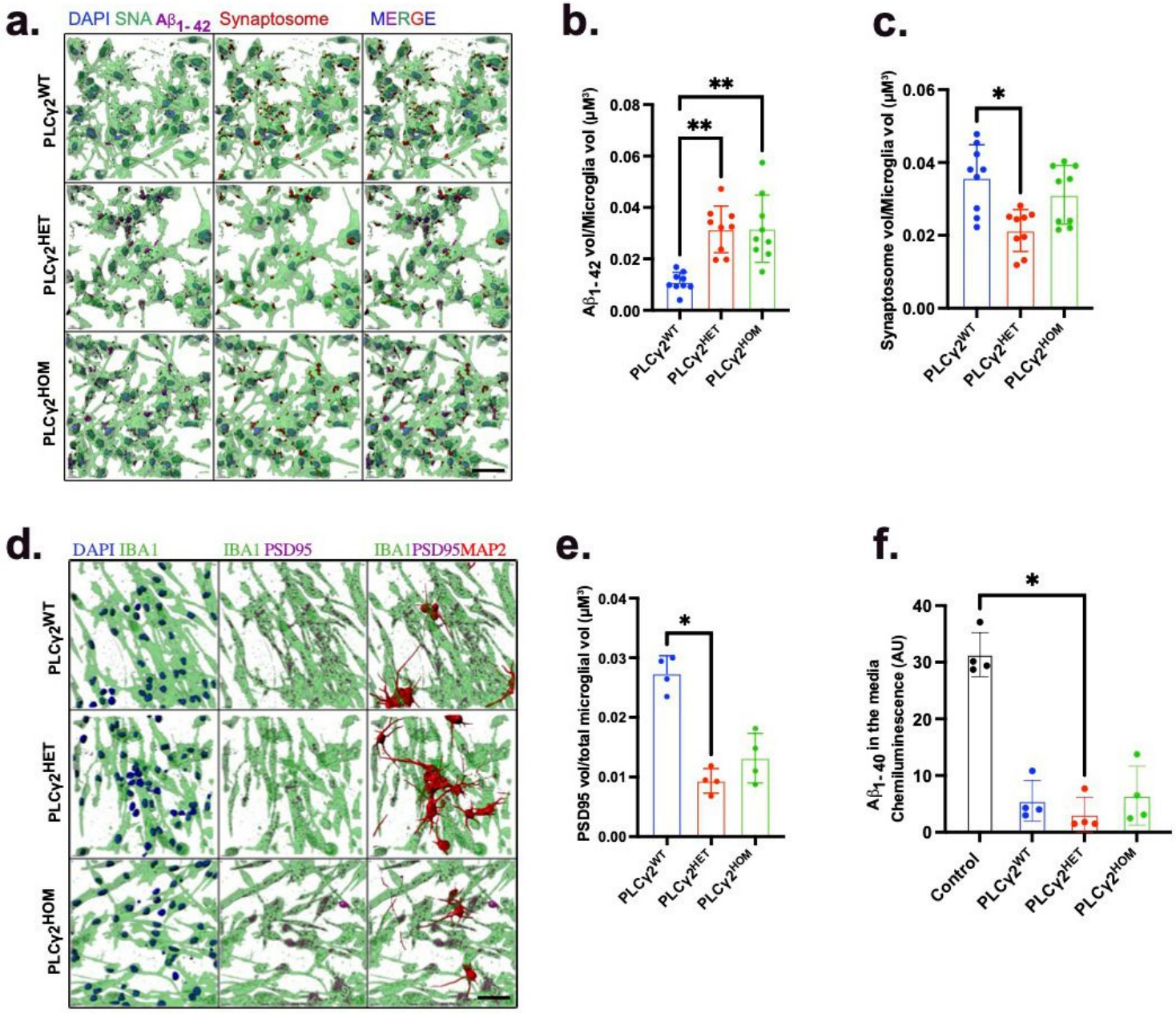

Figure 2

PLCg2^{P522R} reduces synaptic pruning in hiPSC derived cortical neuron and microglia co-culture.

a-c, IMARIS 3D reconstruction analysis of Ab_{1-42} HyLite Fluor 647 (magenta) and tdTomato-synaptosome (red) uptake in PLCg2^{WT}, PLCg2^{HET} and PLCg2^{HOM} hiPSC derived microglia following incubation with both cargoes concurrently. Data is expressed as a proportion of total cell volume, calculated using SNA (Sambucus Niagra Lectin) staining (green). **d-e**, IMARIS 3D reconstruction analysis of synapse uptake by PLCg2^{WT}, PLCg2^{HET} and PLCg2^{HOM} hiPSC derived microglia in neuronal-microglial co-culture. Synaptic

elements within microglia were detected using PSD-95 immunofluorescence (magenta), microglia cells were identified using Iba1 (green), and iPSC derived cortical neurons were visualised using MAP2 (red). Synaptic uptake was expressed as a proportion of total microglial cell area (e). **f,** electrochemiluminescence quantification of Ab_{1-40} levels in media harvested from microglia-neuronal co-culture plates. Ab_{1-40} release into the media from cortical neurons was also assessed in the absence of microglia (control). Data is expressed as chemiluminescent signal intensity. All data is presented as mean ± SD and was analysed using the Kruskal-Wallis with Dunns multiple comparisons test. (*p<0.05, **p<0.01, n=3-4, Scale bar 50mM).

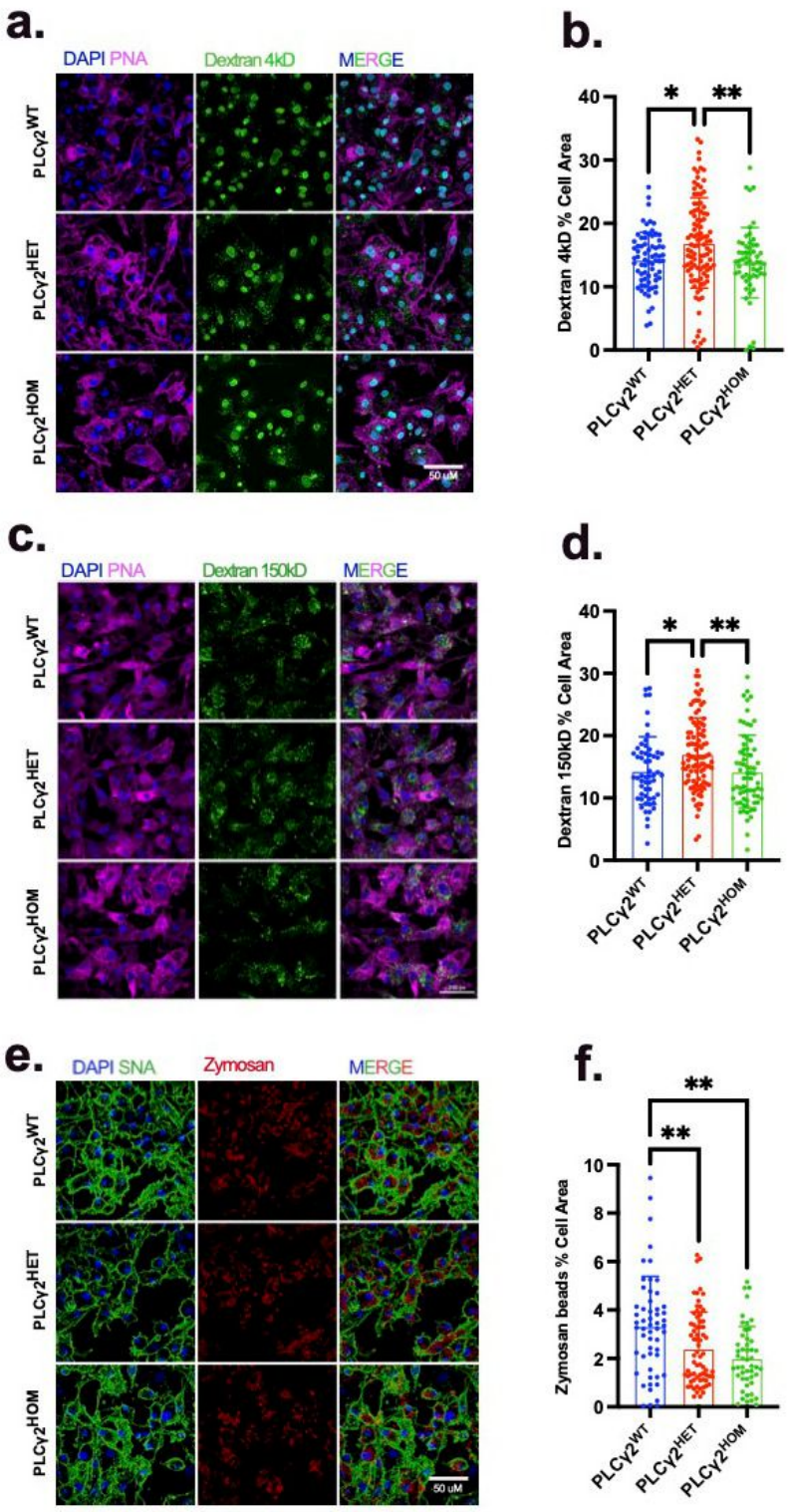

Figure 3

PLCg2^{P522R} modulation of cargo uptake is size dependent.

a-d, Fluorescent confocal analysis of 4kDa (a-b) or 150kDa (c-d) FITC-dextran (green) uptake by PLCg2^{WT}, PLCg2^{HET} and PLCg2^{HOM} hiPSC derived microglia. Internalised dextran is expressed as a proportion of total cell area, detected using PNA (Peanut Agglutinin) stain (magenta). **e-f,** Fluorescent confocal analysis

of Alexa Fluor™ 594-zymosan A Bioparticles™ (red) uptake by PLCg2^{WT}, PLCg2^{HET} and PLCg2^{HOM} hiPSC derived microglia. Internalised zymosan particles are expressed as a proportion of total cell area, detected using SNA stain (green). All data is presented as mean ± SD and was analysed using the Kruskal-Wallis with Dunns multiple comparisons test. (*p<0.05, **p<0.01, n=3, Scale bar 50mM).

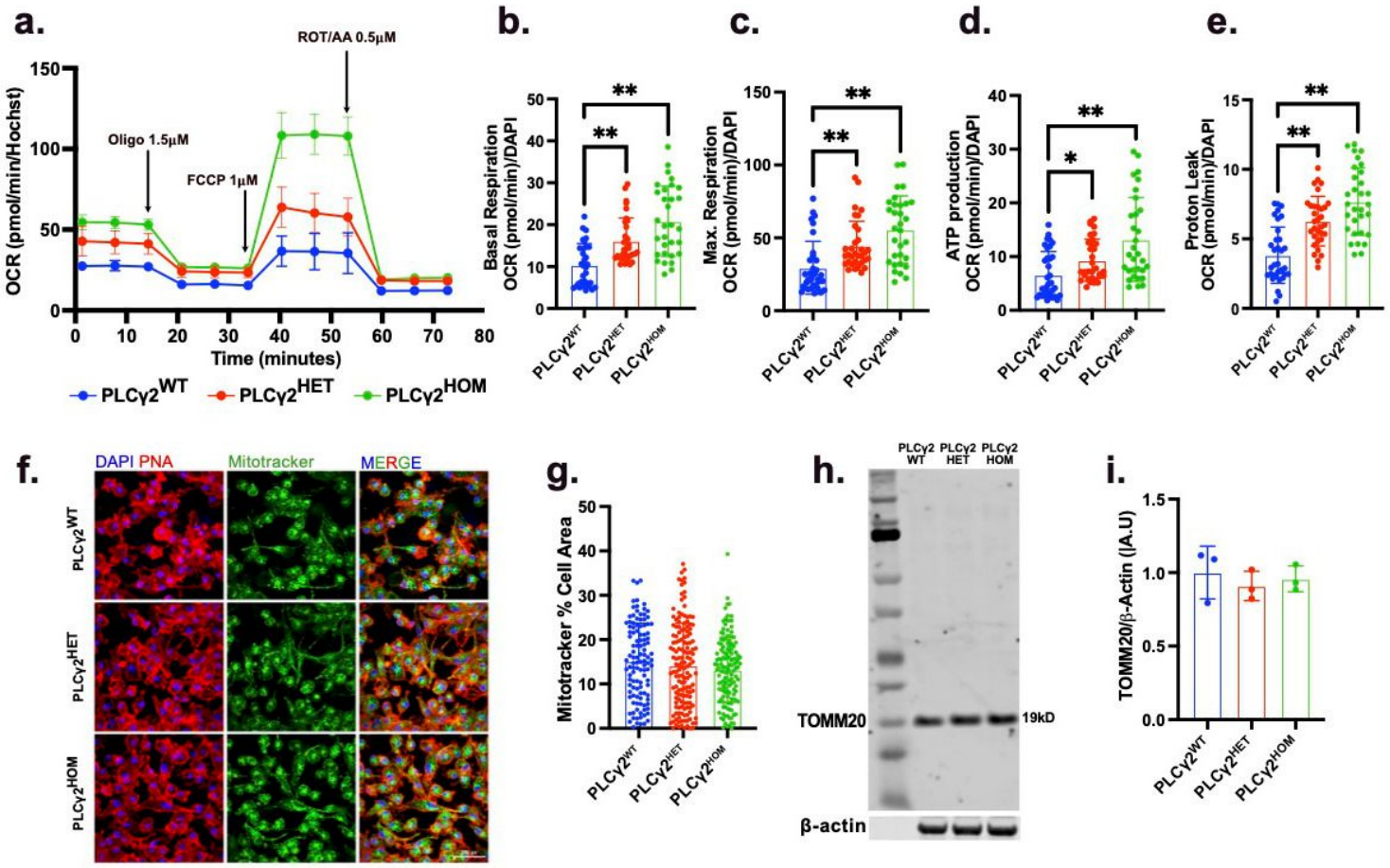

Figure 4

PLCg2^{P522R} modulates expression of a number of microglial genes.

a, Heatmap demonstrating expression fold-changes detected vis qPCR analysis in selected genes in PLCg2^{WT}, PLCg2^{HET} and PLCg2^{HOM} hiPSC derived microglia. **b,** Table showing the qPCR derived median CT value and interquartile range indicating the relative expression of selected genes in PLCg2^{WT}, PLCg2^{HET} and PLCg2^{HOM} hiPSC derived microglia, and the respective p values obtained following Kruskal-Wallis with Dunns multiple comparisons test analysis for each gene. (*p<0.05, **p<0.01, n=7).

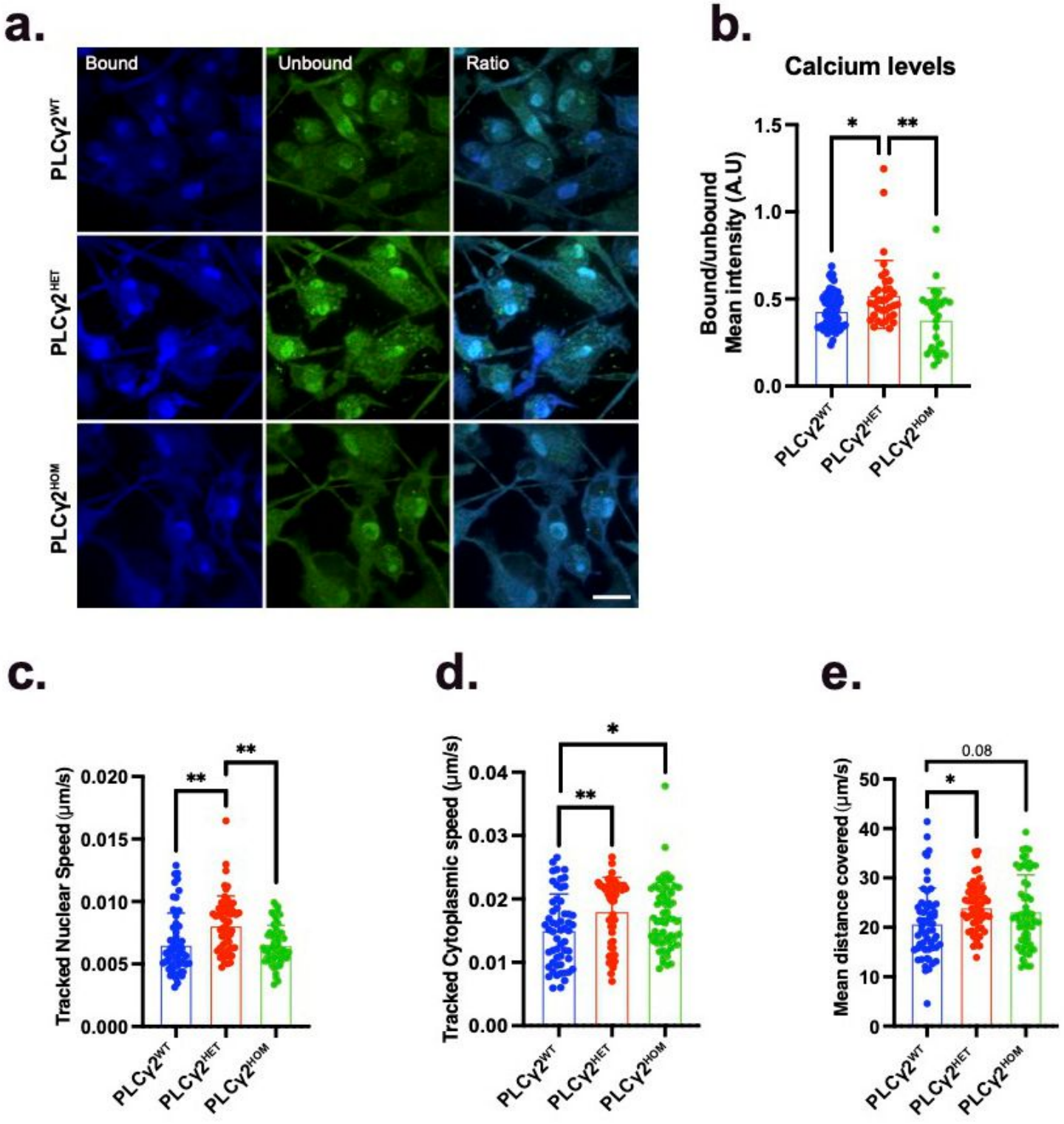

Figure 5

PLCg2^{P522R} modulates mitochondrial activity but not abundance.

a-e, Real time oxygen consumption rate (OCR) at baseline and in response to oligomycin (ATP-synthase inhibitor), FCCP (mitochondrial membrane uncoupler) and rotenone/antimycin-A (Complex I and III inhibitors) in PLCg2^{WT}, PLCg2^{HET} and PLCg2^{HOM} hiPSC derived microglia. Calculated basal respiration

(b), maximal respiration (c) ATP production (d) and proton leak (e) are reported. **f-g,** Fluorescent confocal analysis of mitochondrial abundance in PLCg2^{WT}, PLCg2^{HET} and PLCg2^{HOM} hiPSC derived microglia. Mitochondria were visualised using MitoTracker Green^{FM} (green), and expressed as a proportion of total cell area, detected using PNA stain. Data is presented as mean ± SD and was analysed using the Kruskal-Wallis with Dunns multiple comparisons test. **h-i,** Western blot analysis of mitochondrial protein TOMM20 in PLCg2^{WT}, PLCg2^{HET} and PLCg2^{HOM} hiPSC derived microglia. Expression levels were normalised to b-actin. Data is presented as mean ± SD and analysed using one-way ANOVA with the Tukey multiple comparisons test. (*p<0.05, **p<0.01, n=3-4. Scale bar 50mM).

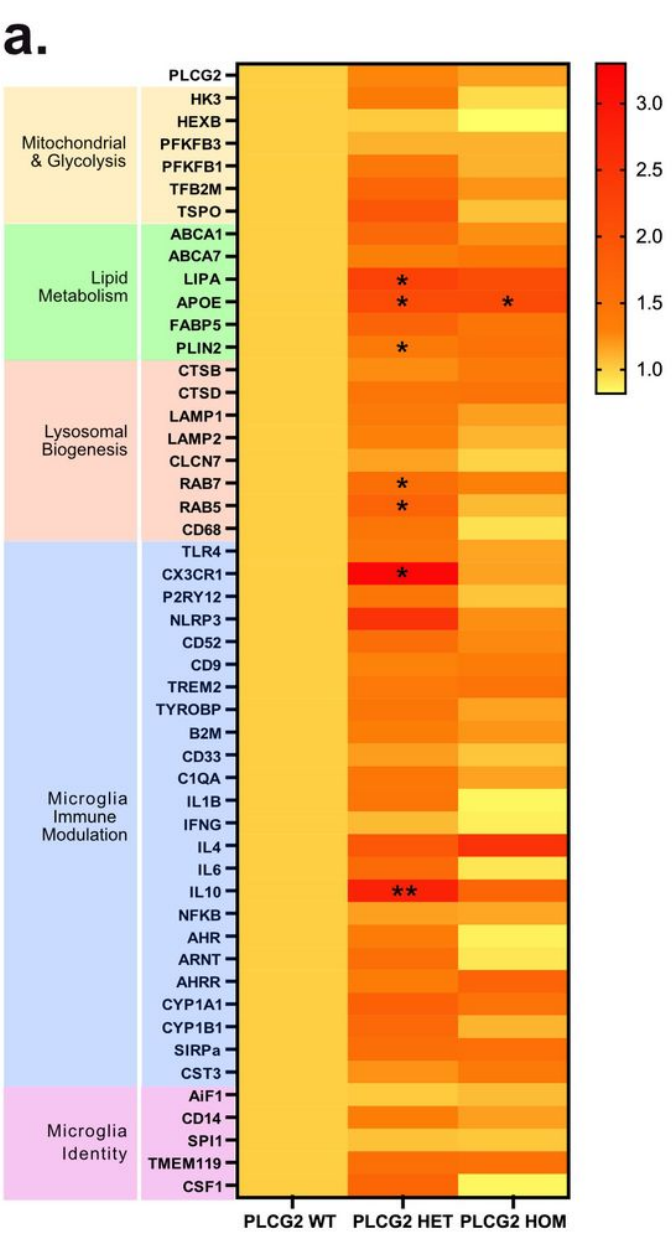

b.

	Median CT Value (Interquartile range)			P value		
	PLCG2 WT	PLCG2 HET	PLCG2 HOM	WT Vs HET	WT Vs HOM	HET Vs HOM
PLCG2	0.87 (0.57)	1.28 (1.37)	1.18 (0.56)	0.43	1.00	0.79
HK3	1.02 (0.23)	1.37 (0.92)	0.95 (0.77)	0.27	1.00	0.10
HEXB	0.95 (0.53)	1.02 (2.85)	0.82 (0.45)	0.84	1.00	1.00
PFKFB3	1.64 (0.48)	1.11 (0.51)	1.11 (0.61)	0.57	0.84	1.00
PFKFB1	0.57 (0.97)	1.42 (0.91)	1.11 (0.75)	0.84	1.00	1.00
TFB2M	1.07 (0.41)	1.70 (2.53)	1.22 (0.91)	0.47	1.00	1.00
TSPO	1.06 (1.84)	1.95 (1.04)	1.05 (0.93)	0.43	1.00	0.63
ABCA1	0.87 (0.84)	1.65 (1.82)	1.24 (0.86)	0.21	1.00	0.90
ABCA7	0.75 (3.80)	1.31 (1.78)	1.43 (1.93)	1.00	1.00	1.00
LIPA	1.12 (0.20)	2.27 (2.07)	2.10 (2.31)	***0.03**	0.50	0.79
APOE	1.24 (0.65)	2.12 (1.55)	2.14 (2.84)	***0.03**	***0.03**	1.00
FABP5	1.59 (1.63)	1.72 (1.06)	1.45 (0.77)	1.00	1.00	1.00
PLIN2	1.11 (0.38)	1.38 (0.19)	1.52 (0.66)	***0.04**	0.12	1.00
CTSB	1.16 (0.47)	1.25 (1.84)	1.39 (0.97)	0.97	1.00	1.00
CTSD	1.05 (0.91)	1.46 (1.54)	1.49 (0.72)	0.66	1.00	1.00
LAMP1	1.34 (1.29)	1.39 (1.53)	1.18 (0.67)	1.00	1.00	1.00
LAMP2	1.01 (1.40)	1.30 (2.08)	1.10 (1.38)	0.97	1.00	1.00
CLCN7	1.05 (1.23)	1.17 (1.03)	0.98 (0.73)	1.00	1.00	1.00
RAB7	1.01 (0.52)	1.56 (2.22)	1.30 (1.66)	***0.03**	0.36	1.00
RAB5	1.00 (0.05)	1.73 (2.28)	1.08 (1.08)	***0.017**	1.00	0.17
CD68	1.01 (0.39)	1.46 (1.76)	0.93 (1.33)	0.17	1.00	0.57
TLR4	0.94 (1.58)	1.38 (2.19)	1.16 (2.22)	0.30	1.00	1.00
CX3CR1	0.78 (1.39)	3.19 (3.16)	1.17 (1.81)	***0.04**	1.00	0.12
P2RY12	0.96 (0.50)	1.46 (2.04)	1.04 (2.48)	0.17	1.00	0.43
NLRP3	0.95 (0.48)	2.51 (2.28)	1.24 (0.79)	0.15	1.00	0.76
CD52	1.24 (2.85)	1.58 (6.40)	1.26 (2.08)	0.82	1.00	1.00
CD9	0.34 (4.44)	1.29 (2.23)	1.35 (2.18)	0.28	1.00	0.66
TREM2	1.02 (1.83)	1.42 (3.85)	1.50 (3.39)	0.63	1.00	1.00
TYROBP	1.03 (0.50)	1.45 (1.46)	1.17 (1.30)	0.47	1.00	1.00
B2M	0.81 (3.64)	1.33 (1.11)	1.22 (0.60)	1.00	1.00	1.00
CD33	1.06 (0.65)	1.19 (0.46)	1.04 (1.03)	1.00	1.00	1.00
C1QA	1.35 (1.28)	1.43 (1.77)	1.17 (1.16)	1.00	1.00	1.00
IL1B	1.20 (1.62)	1.47 (0.97)	0.85 (0.80)	0.50	1.00	0.43
IFNG	0.97 (0.30)	1.08 (2.44)	0.88 (1.64)	0.36	1.00	0.36
IL4	1.23 (5.37)	1.92 (1.49)	2.52 (2.34)	0.63	0.55	1.00
IL6	1.06 (0.28)	1.63 (2.49)	0.91 (1.53)	0.63	1.00	0.55
IL10	0.97 (1.62)	2.79 (10.9)	1.70 (2.11)	****0.0017**	1.00	0.08
NFKB	0.98 (0.46)	1.18 (1.57)	1.15 (0.76)	0.41	1.00	0.66
AHR	0.88 (0.42)	1.36 (2.56)	0.87 (0.82)	0.82	1.00	0.28
ARNT	0.77 (4.13)	1.56 (1.65)	0.91 (0.93)	1.00	1.00	1.00
AHRR	0.70 (2.12)	1.35 (1.08)	1.73 (1.37)	1.00	1.00	1.00
CYP1A1	1.31 (2.91)	1.78 (8.06)	1.01 (1.69)	0.12	1.00	0.36
CYP1B1	1.02 (0.26)	1.66 (0.96)	1.10 (0.87)	0.12	1.00	0.63
SIRPa	0.98 (0.42)	1.56 (1.40)	1.54 (1.00)	0.32	0.18	1.00
CST3	0.84 (0.51)	1.23 (1.01)	1.39 (1.06)	0.79	1.00	1.00
AiF1	1.06 (0.82)	1.02 (1.07)	1.07 (0.96)	1.00	1.00	1.00
CD14	1.25 (1.20)	1.33 (1.99)	1.18 (1.04)	1.00	1.00	1.00
SPI1	1.06 (0.42)	1.05 (1.16)	1.03 (0.75)	1.00	1.00	0.87
TMEM119	0.78 (0.79)	1.56 (3.99)	1.52 (2.91)	0.17	0.25	1.00
CSF1	1.64 (1.30)	1.71 (1.68)	0.85 (0.73)	1.00	1.00	0.90

Figure 6

PLCg2 ^{P522R} modulates basal Ca^{2+} levels and microglial motility.

a-b, Fura Red^{TM} ratiometric analysis of bound vs. unbound Ca^{2+} levels in PLCg2^{WT}, PLCg2^{HET} and PLCg2^{HOM} hiPSC derived microglia. **c-e,** Cellular motility assay assessing whole cell motility (nuclear tracking; c) and microglial ramification and surveillance (cytoplasmic tracking; d) as well as associated distance travelled (e) in PLCg2^{WT}, PLCg2^{HET} and PLCg2^{HOM} hiPSC derived microglia. All data is presented as mean ± SD and was analysed using the Kruskal-Wallis with Dunns multiple comparisons test. (*p<0.05, **p<0.01, n=4-6, Scale bar 50mM).

Supplementary Files

This is a list of supplementary files associated with this preprint. Click to download.

- Graphicalabstract.jpg
- SupplementaryData.docx